AFRL-SR-AR-TR-06-0460

REPORT DOCUMENTATION PAGE

1. REPORT DATE (DD-MM-YYYY)	2. REPORT TYPE	3. DATES COVERED (From - To)
01-09-2006	Final Technical Report	02-01-2003 – 5-31-2006

4. TITLE AND SUBTITLE
Advanced Stimulated Scattering Measurements in Supercritical Fluids

5a. CONTRACT NUMBER
F49620-03-C-0015

5b. GRANT NUMBER

5c. PROGRAM ELEMENT NUMBER
61102F

6. AUTHOR(S)
Gregory W. Faris

5d. PROJECT NUMBER
2308

5e. TASK NUMBER
BX

5f. WORK UNIT NUMBER

7. PERFORMING ORGANIZATION NAME(S) AND ADDRESS(ES)

SRI International
333 Ravenswood Avenue
Menlo Park, CA 94025-3493

8. PERFORMING ORGANIZATION REPORT NUMBER
MP 06-029

9. SPONSORING / MONITORING AGENCY NAME(S) AND ADDRESS(ES)
AFOSR/NA
875 Randolph Street
Suite 325, Room 3112
Arlington, VA 22203
Dr Julian Tishkoff

10. SPONSOR/MONITOR'S ACRONYM(S)

11. SPONSOR/MONITOR'S REPORT NUMBER(S)

12. DISTRIBUTION / AVAILABILITY STATEMENT

Approved for public release; distribution is unlimited

13. SUPPLEMENTARY NOTES

14. ABSTRACT

Work was performed on development of stimulated Brillouin and Rayleigh scattering for measurements in supercritical fluids. Improvements were made to our instrumentation to fully resolve the stimulated Rayleigh scattering peak in the supercritical regime, a capability that is important for measurement of the thermal properties of supercritical fuels. To provide narrower linewidths, the injection-seeded laser has been modified to operate as a pulse-amplified system. A new electronic modulation technique has been developed to further improve our ability to measure the Rayleigh peak. This method used a single laser source, eliminating the drift problems of the two laser method and improving the frequency offset accuracy. Interesting structure was observed with stimulated Brillouin scattering in the supercritical regime indicating that the liquid-gas phase boundary continues above the critical point.

15. SUBJECT TERMS
Supercritical fluids, stimulated scattering, Brillouin scattering, Rayleigh scattering, elastic properties, thermal properties

16. SECURITY CLASSIFICATION OF:			17. LIMITATION OF ABSTRACT	18. NUMBER OF PAGES	19a. NAME OF RESPONSIBLE PERSON
a. REPORT	b. ABSTRACT	c. THIS PAGE			Julian M. Tishkoff
Unclassified	Unclassified	Unclassified	UL	48	19b. TELEPHONE NUMBER (include area code) (703) 696-8478

Standard Form 298 (Rev. 8-98)
Prescribed by ANSI Std. Z39.18

Final Report • September 2006

ADVANCED STIMULATED SCATTERING MEASUREMENTS IN SUPERCRITICAL FLUIDS

Prepared by:

Gregory W. Faris
Molecular Physics Laboratory

SRI Project 12446

Contract Number F49620-03-C-0015

MP 06-029

Prepared for:

Air Force Office of Scientific Research
AFOSR/NA
875 Randolph Street
Suite 325, Room 3112
Arlington VA 22203

Attn: Dr. Julian Tishkoff

TABLE OF CONTENTS

OBJECTIVES

The objectives of this research are to develop stimulated scattering as a diagnostic for supercritical fluids and use this technique to improve our understanding of fluids in the supercritical state.

The study of supercritical fluids and flows requires new diagnostic techniques. Currently available techniques such as laser-induced fluorescence (LIF) and coherent anti-Stokes Raman scattering (CARS) are complicated at high pressures by increased molecular interactions, leading to stronger quenching, larger absorption and refractive index, and incomplete understanding of the influence of local conditions on spectroscopic parameters such as linewidths, nonresonant background contributions, and quenching rates. By comparison, application of stimulated scattering techniques to supercritical fluids is relatively straightforward.

STATUS OF EFFORT

Work was performed on development of stimulated Brillouin and Rayleigh scattering for measurements in supercritical fluids. Improvements were made to our instrumentation to fully resolve the stimulated Rayleigh scattering peak in the supercritical regime, a capability that is important for measurement of the thermal properties of supercritical fuels. To provide narrower linewidths, the injection-seeded laser has been modified to operate as a pulse-amplified system. A new electronic modulation technique has been developed to further improve our ability to measure the Rayleigh peak. This method used a single laser source, eliminating the drift problems of the two-laser method and improving the frequency offset accuracy. Interesting structure was observed with stimulated Brillouin scattering in the supercritical regime indicating that the liquid-gas phase boundary continues above the critical point.

ACCOMPLISHMENTS / NEW FINDINGS

SUMMARY / OVERVIEW

This project uses stimulated Rayleigh and Brillouin scattering as a tool to investigate supercritical fluids. From the measurements, we can determine thermal, compressional, and compositional properties of supercritical fuels in situ. This research effort addresses the need for new diagnostics in the study of the supercritical and near-critical regimes, where low-pressure diagnostics do not work well.

INTRODUCTION

Supercritical fuels and mixing are of increasing importance for Air Force projects such as advanced air-breathing propulsion systems and advanced launch boosters. The relative lack of experience with, and understanding of, the fluid properties, fluid dynamics and mixing, and chemical kinetics under such conditions requires the development and application of diagnostic techniques that are able to characterize the new features and processes that may occur. Developing these new techniques will be especially important because existing diagnostic approaches used at low pressures cannot be easily adapted to supercritical conditions. Supercritical conditions are important in two significant areas: For air-breathing propulsion, increasing demands are being placed on fuel as a coolant for the engine, environmental control systems, electronics, and, at high Mach numbers, even the airframe. Together, these cooling needs will heat the fuel to the supercritical phase. Relatively little is known, however, about the properties of fuels in the supercritical regime or the effects of injecting supercritical fuel into subcritical turbines or ramjets. Therefore, new diagnostic approaches are required to understand the state and properties of the fuel as it is heated and to help understand the effects of these supercritical fuels on engine performance.

For high-pressure rocket propulsion, fuel or oxidant may transform from a subcritical to a supercritical state during injection into the combustion chamber. For example, in liquid oxygen-hydrogen rockets, liquid oxygen is injected at supercritical pressure and subcritical temperature and heated to supercritical temperature in the combustion chamber. Improved diagnostics are required to study the significance of this transcritical mixing on rocket engine performance.

High temperatures create many unusual problems for fuel systems. Thermal cracking changes fuel properties and can produce gums and solids that freeze valves and foul fuel nozzles

and heat exchangers. In the supercritical regime, fuels have liquid-like densities and gas-like diffusivities and viscosities. The changing heat load during the flight of advanced aircraft will lead to widely varying fuel properties during a mission; fuel systems must perform well under all these conditions. In the region of the critical point, destructive flow and pressure instabilities can arise. These various effects demand thorough investigation of proposed fuels and fuel systems under anticipated conditions.

TECHNICAL DISCUSSION

Stimulated Scattering

Rayleigh, Brillouin, and Raman scattering occur commonly as spontaneous scattering. Rayleigh scattering results from refractive index variations due to thermal waves or diffusive density fluctuations and compositional fluctuations. Brillouin scattering results from refractive index variations due to sound waves or traveling density or pressure fluctuations. These scattering processes that arise from natural oscillation modes of materials can be used to determine the physical parameters responsible for those oscillations. When these collective modes are excited with a powerful laser, the mode oscillations can be driven so hard that they grow exponentially. In this case, the oscillations cause stimulated scattering. The dominant advantage of stimulated scattering is that the scattered signal can be made arbitrarily large; otherwise, these processes produce extremely weak signals. By using a probe beam to measure the induced amplification, we can obtain very good quantitative results. This technique is distinct from the stimulated scattering that builds up from noise, in which case quantification is very difficult.

The large signals from stimulated scattering are particularly helpful for investigating Rayleigh and Brillouin scattering, where the weak signals available from spontaneous scattering are difficult to discriminate from background excitation light. Other advantages of stimulated scattering include excellent temporal resolution, improved spectral resolution, and higher signal-to-noise ratio. Furthermore, the use of two laser beams allows spatial registration and point measurement of local conditions. Stimulated Rayleigh, Brillouin, and Raman processes together provide measurements of a wide range of material properties. Rayleigh scattering provides information on thermal properties, Brillouin scattering on compressional or elastic properties, and Raman scattering on chemical and compositional properties, density, and temperature. The laser requirements for our stimulated Rayleigh and Brillouin measurements are quite modest. For our two-laser experiments, the pump beam energy is only ~20 μJ, and the probe beam is

provided by a diode laser. Thus, stimulated scattering could be used even as an onboard monitor of fuel state and properties.

Parameters currently of interest to the Air Force for supercritical fuels include compressibility, sonic velocity, density and phase, and chemical composition.[1] All of these parameters can be measured directly by stimulated scattering measurements. Thus, stimulated scattering will play a very important role in understanding fuel performance and in diagnosing fuel system performance—critical steps in assuring the performance of next-generation aircraft. SRI is one of only a handful of groups that have performed stimulated Rayleigh and Brillouin experiments, and, to the best of our knowledge, we are the only group applying these techniques to supercritical fluids.

Transient Grating Techniques

The physical processes involved in stimulated Rayleigh and Brillouin scattering also are involved in transient grating or forced scattering techniques.[2-7] In these techniques, two pulsed laser beams are overlapped to produce a grating. The grating can be produced through either electrostriction or absorption. The grating produces both acoustic and nonpropagating entropy waves, which, when probed by a third laser beam, can provide information about elastic and thermal properties. For the transient grating approach, the grating is produced transverse to the probe beams; for the stimulated scattering method, the grating is longitudinal. The transient grating techniques require phase matching between the three beams so that the Bragg condition is met between the grating and the probe beam. The stimulated scattering approach we use has only two beams, and the phase matching condition is satisfied automatically at every angle and pump wavelength—conditions that make the approach easier to implement. Grating measurements are performed using pulsed lasers. With the frequency modulation techniques we are developing, it may be possible to perform stimulated scattering measurements with CW diode lasers.

Experiment

We perform stimulated scattering measurements by producing strong scattering interactions using a pump laser and then probing the scattering with a second probe laser. The pump laser we use is an injection-seeded Nd:YAG laser, and the probe laser is a tunable diode laser. The pump laser sets up an electric polarization oscillating at the characteristic frequency of a scattering mode of the material.[8] For strong laser driving, this polarization acts as a driving force, leading to amplification of both the material oscillation and the scattered optical wave. The optical amplification is detected as a gain or loss on the probe beam. The overlap volume of

the pump and probe beams determines the spatial resolution. The stability of the probe and pump lasers has been optimized to allow for more reliable operation and narrower bandwidth, respectively. We have constructed a high-pressure cell suitable for measurements in the supercritical and near-critical regions.

Examples of stimulated Rayleigh / Brillouin scattering spectra measured at 1064 nm in n-hexane near the critical temperature at three different pressures are shown in Fig. 1. The critical point for n-hexane occurs at a pressure of 30.3 bar and temperature of 234 °C.[9] The peaks to the left and right of each spectrum are the gain and loss Brillouin peaks, respectively. The central peak is the stimulated Rayleigh peak. Optical absorption enhances the Rayleigh peak and produces asymmetry to the Brillouin peaks. Also shown in Fig. 1 are fits to the data. The electrostrictive Brillouin lineshape is described by the real part of the complex Lorentzian profile; the thermal Brillouin and Rayleigh lineshapes are described by the imaginary parts of a complex Lorentzian profile.[8,10] The measured lineshapes are given by the convolution of the Gaussian spectral lineshape of the Nd:YAG pump laser with these Lorentzian profiles. The following figures present stimulated Brillouin scattering properties for n-hexane at 1064 nm at sub-, near-, and supercritical conditions. Additional information on the measurements and experimental apparatus is presented in the manuscript included in the appendix.

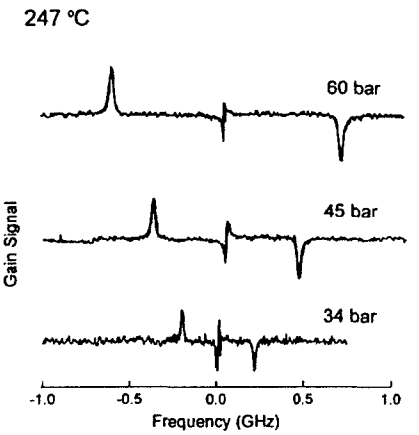

Fig. 1. Stimulated scattering spectra at 1064 nm for three different pressures.

Figures 2 and 3 present three-dimensional views of the Brillouin shifts and the Brillouin peak widths observed for n-hexane at 1064 nm in a wide range of temperature and pressure conditions. In both graphs, an open circle on the plane of the temperature-pressure coordinate system indicates the location of the critical point for n-hexane. The solid points correspond to the extracted values from our fits to the data. In both graphs, the scatter of the data points is representative of the experimental uncertainties. The uncertainty of the fit (one standard deviation) is typically 1 % and 5 % for the Brillouin shift and Brillouin peak width, respectively; however, repeated measurements at the same conditions show reproducibility to within approximately 10 % and 20 % for the Brillouin shift and width, respectively. The main source of experimental errors is the (unavoidable) existence of temperature and pressure fluctuations of the fluid under study. Our experiments for conditions ranging from ambient temperature and pressure to the supercritical state have shown clearly that these fluctuations become dramatically

larger as the system approaches the critical point. The mesh surfaces shown in Figs. 2 and 3 have been created by numerical interpolation through the experimental points using commercially available software (Sigmaplot by SPSS Inc.). They are presented as a visual aid to the identification of trends in the experimental data. In both Figs. 2 and 3, the magnitude of the Brillouin shift and width exhibits a minimum in the region of the critical point. This observation is consistent with extreme values of the speed of sound and the acoustic damping rate attained near or at the critical point. We note that although our apparatus is successful in recording reliable spectra very close to the critical point, a limit exists within approximately a couple of bar and degrees centigrade, where critical opalescence and fluid fluctuations make measurements impossible. Consequently, the magnitude of the Brillouin shift and width could reach smaller values and even zero at the critical point.

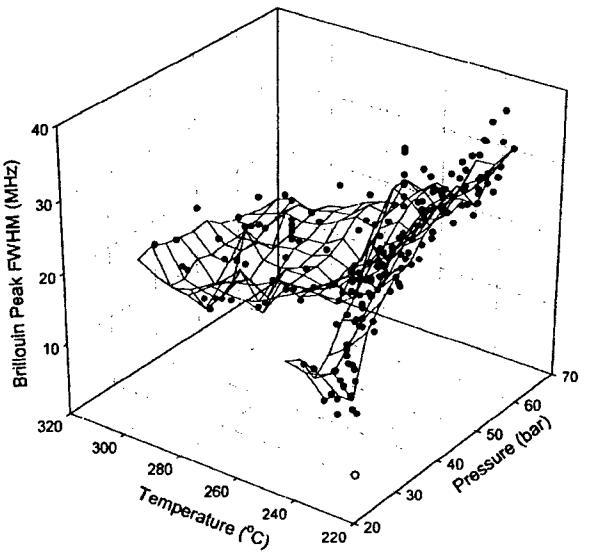

Fig. 2. Three-dimensional plot of stimulated Brillouin scattering widths.

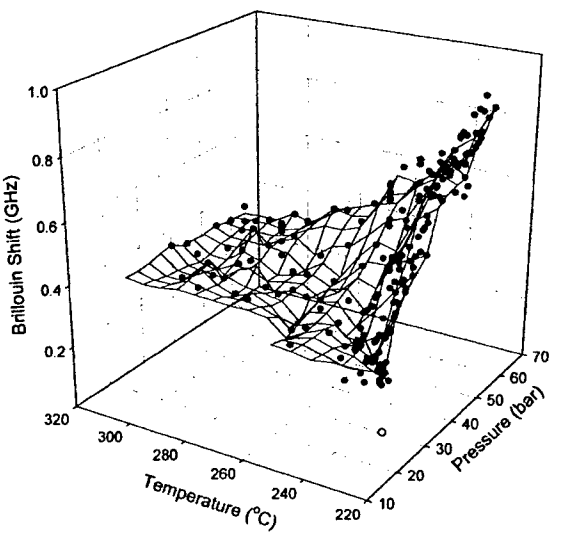

Fig. 3. Three-dimensional plot of stimulated Brillouin scattering shifts.

Figures 4 and 5 show two-dimensional cross sections through the graphs of Figs. 2 and 3 that present a clearer view of the behavior of the Brillouin shift and Brillouin peak width as a function of temperature and pressure. The error bars shown for the Brillouin width correspond to one standard deviation, as extracted from the fits to the data. In the case of the Brillouin shift the error bars from the fit to the data are comparable to the size of the point markers.

Comparison with theory of the widths, shifts, and heights of the electrostrictive Brillouin, thermal Brillouin, and thermal Rayleigh peaks has shown consistency of the theory through the relationships between the heights and widths of the thermal Brillouin and thermal Rayleigh

peaks. A remarkable feature in the Brillouin and Rayleigh measurements is the discontinuity in the observed properties that occurs near the critical point, as shown in the figures presented above.

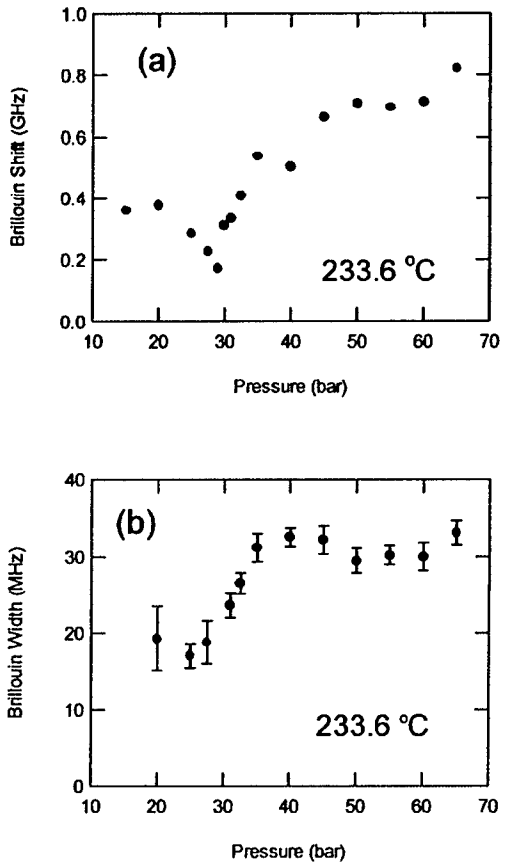

Fig. 4. Effect of pressure on Brillouin shift and width.

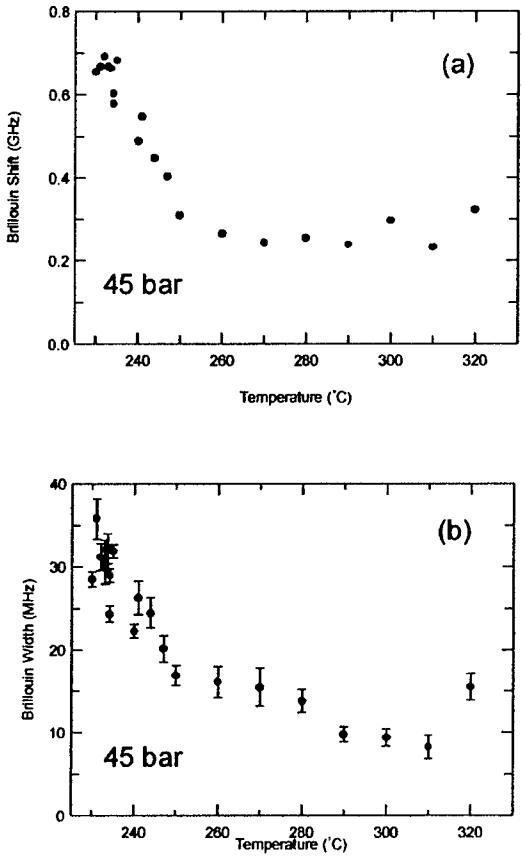

Fig. 5. Effect of temperature on Brillouin shift and width.

Figure 6 shows results from analysis of the intensities of the stimulated Brillouin peaks. Both the absorptive and the electrostrictive components of the Brillouin scattering peak show a sharp discontinuity near the critical point. This discontinuity is expected because the near critical fluid is very susceptible to density fluctuations such as those induced by stimulated Brillouin scattering. The same trend occurs in the absorptive component.

Extrapolated Phase Boundary

We have made an interesting observation regarding our stimulated scattering measurements in the supercritical regime. The Brillouin shifts, Brillouin widths, and Brillouin peak heights show structure above the critical point. The structure is most prominent in the

Brillouin peak heights. For each measurement temperature, there is a pressure at which the Brillouin peak height is greatly enhanced (see, e.g., Fig. 6). As shown in Fig. 7, when we plot the pressure of the enhanced Brillouin peak as a function of temperature, we find that the points fall directly on the extrapolation of gas-liquid equilibrium curve as calculated using a Wagner equation and the vapor pressure data for n-hexane.[9] The data of Fig. 7 indicates that the liquid/gas phase boundary continues in some form well into the supercritical regime even though the separate phases no longer exist. Measurements using other techniques support the existence of this extrapolated phase boundary.[11,12]

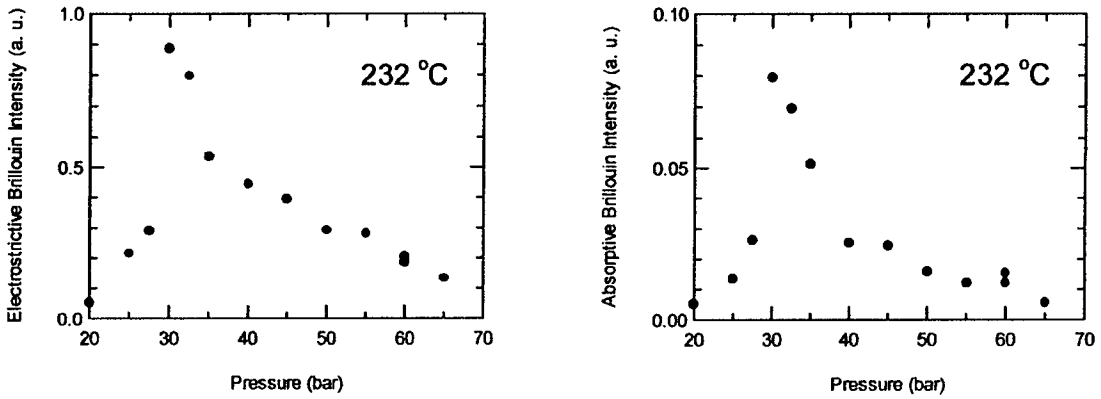

Figure 6. The electrostrictive and absorptive Brillouin peak intensity observed in stimulated Brillouin scattering for n-hexane at 240°C as a function of pressure.

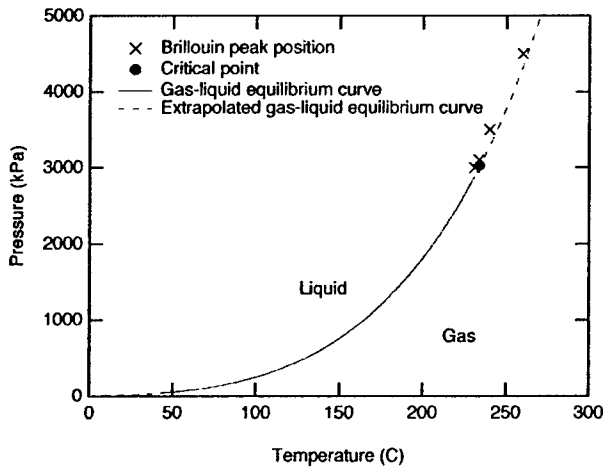

Figure 7. Pressure-temperature phase diagram showing Brillouin peak positions.

Refractive Index Measurements

To provide the most accurate physical property measurements, we must know the refractive index. We have evaluated a number of methods for refractive index measurement,

including beam translation, interferometric, and beam deflection methods. We prefer the beam deflection method because it provides larger signals than the beam translation method and is simpler to implement than the interferometric methods. RF modulation techniques may offer another method for refractive index measurement.

Narrowband Pump Laser

One challenge for making measurements in the supercritical region is that the Rayleigh peak becomes extremely narrow. In hexane, the Rayleigh peak is about 7 MHz at room temperature, but drops to values of a few megahertz at elevated temperatures and pressures. The linewidth of the tunable diode laser that we use as a probe laser is not an issue. Although no active frequency stabilization is applied, it produces a linewidth of less than 300 kHz in 50 ms. However, the pump laser has important linewidth limitations due to the pulsewidth and the injection-seeding dither. The pump laser cavity is locked to the injection-seeding ring laser by dithering the pump laser cavity length with feedback stabilization to minimize the Q-switch buildup time. This dither corresponds to an alternating frequency shift of approximately 10 MHz on every other pulse. We prevent the dither from limiting the linewidth of the stimulated scattering measurements by acquiring the data at 5 Hz (i.e., on every other pulse). The pump laser also has a linewidth contribution related to the Fourier transform relationship between the pulsewidth in the time domain and the linewidth in the frequency domain. We can reduce this linewidth by lowering the cavity gain to produce long pulse lengths. We typically operate the pump laser with a pulsewidth of about 30 ns, which corresponds to a Fourier transform-limited linewidth of 15 MHz. A linewidth contribution is also made by the relative frequency drift between the pump and probe lasers. We have corrected for this drift by measuring the frequency of the heterodyne beat signal obtained by mixing a portion of the seed laser beam with a portion of the probe laser beam. We then use the heterodyne frequency to provide a corrected frequency axis for the stimulated scattering spectrum.

We investigated methods to simplify the laser apparatus and improve the linewidth performance. Even with the steps taken to minimize the contributions from the injection-locking dither and pump-probe frequency drift, we still have the transform-limited pump laser linewidth of 15 MHz, which is significantly broader than the narrowest Rayleigh linewidths of a few megahertz. Fortunately, the stimulated Rayleigh and Brillouin measurements require relatively low pump powers. To obtain gain signals of the order of 1%, we require pump energies of tens of microjoules, or peak powers of nearly 1 kW. Thus it is practical to reach the required power levels through direct amplification of our probe laser. We first examined the amplification available from a CW Nd:YAG laser (Coherent Antares system). Although the CW laser provides

a maximum power of only 10 W, with CW measurements we can use lock-in detection or related modulation techniques to measure smaller signals than those that can be measured with the pulsed laser. Furthermore, the Rayleigh peak will be larger when it is fully spectrally resolved, reducing the pump power requirement. We found that the single-pass gain of the CW laser was insufficient to extract the full available power in a small number of amplification passes. Although extraction of the full power would be possible with injection-locked laser operation of the CW laser, we chose to pursue pulsed amplification instead, which can provide higher peak powers and is a smaller departure from our current measurement approach.

Pulse Amplification Systems

As a first step toward pulse amplification, we modified the injection-seeded pump laser to operate as an amplifier rather than a laser. The laser uses two quarter-wave plates to produce circular polarization in the oscillator Nd:YAG rod to minimize multimode operation. Output coupling is obtained from an intracavity polarizer. By removing one of the quarter-wave plates and adjusting the remaining waveplate, we can force the laser cavity to operate as a double-pass amplifier. We modified the layout of the second (amplifier) Nd:YAG rod to serve as a second double-pass amplifier through appropriate insertion of a polarizer, quarterwave plate, and mirror. With this arrangement, we were able to obtain pulse energies of several millijoules. Much higher pulse energies can be obtained by further increasing the flashlamp pump energy. However, at higher energies, amplified spontaneous emission (ASE) occurred in the laser, leading to a broadband contribution to the linewidth. To improve the narrowband laser energy, we used a second Nd:YAG laser (QuantaRay DCR) to amplify the pulses further. A spatial filter was placed between the two lasers to minimize contributions from ASE; however, that approach did not improve the narrowband output energy significantly. We attribute the broadband emission at higher lamp energies to parasitic oscillation from the various optical elements in the primary laser in its original configuration.

To overcome the parasitic oscillations and remaining ASE, we have rebuilt the primary laser completely as a direct double-stage double-pass amplifier (Fig. 8). This configuration has a spatial filter between each stage of amplification and the fewest optical elements in the beam path. The laser rods can generate a single-pass gain of well over 100.[32] Thus the gain is ample for saturating the final amplification stage, which would produce an energy of 1 joule.

A number of optical elements are not shown in Fig. 8. A waveplate and a polarizer are placed between the cw laser and the isolator. The beam split by the polarizer is to be used as a probe beam. Rotation of the waveplate varies the intensities of the probe beam and beam

passing to the amplifier. A second waveplate is placed after the isolator to correct for the partial polarization rotation in the isolator. A telescope beam expander with a magnification of 7.5 is between the second isolator and the high power polarizer used as an output coupler. The spatial filters are built using rod-based cage structures. Threaded mounts on the lenses provide coarse adjustment of the positions of the lenses in the spatial filters. Fine transverse adjustment of the pinholes is provided using x-y lens mounts. Thermal lensing in the laser rods necessitated the addition of longitudinal adjustments on the pinholes as well, provided by translation stages. An additional translation stage was added to the last lens before the retroreflection mirror to allow for precise recollimation for the second pass through the spatial filters and amplifiers.

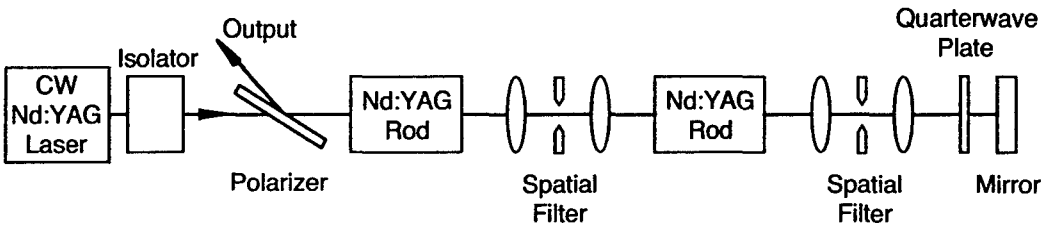

Figure 8. Schematic of pulse-amplified laser.

The temporal profile of the pulse-amplified beam is shown in Fig. 9. The pulse shape follows the shape of the lamp emission. The full width half maximum of the pulse is roughly 170 μs. The transform-limited lower bound for the linewidth of this pulse would be less than 1 kHz, which is far below our target linewidth of ~100 kHz. Peak powers are currently over 40 W with pulse energies of around 10 mJ, limited by parasitic oscillation.

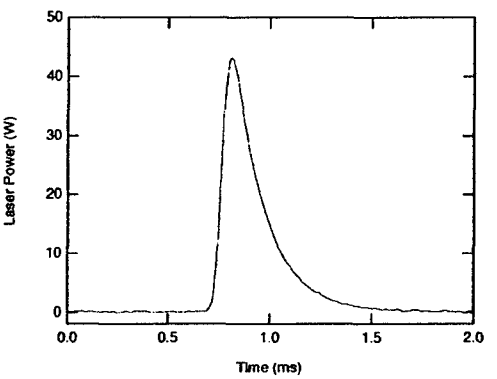

Figure 9. Temporal profile of pulse-amplified laser.

We had been using a diode pumped monolithic Nd:YAG ring laser as the master oscillator for the pulse amplification. This laser is 14 years old, and degradation of the laser led it to operate in a doughnut mode, which was unsuitable for single spatial mode pulse amplification. We substituted an external cavity diode laser for our more recent experiments. The laser produces higher output power (up to 10 mW compared with about 1 mW for the Nd:YAG ring laser), but it has a lower frequency stability. This reduced frequency stability should not be a problem when using the electronic modulation approach described below. The higher output power of the external cavity diode laser did not result in a higher output power from the pulsed amplifier, possibly because the diode laser has a poorer spatial mode.

Frequency Offset Detection

Another factor that affects our ability to resolve the stimulated Rayleigh peak is the relative stability of the pump and probe lasers. Fortunately, the frequency offsets for the Rayleigh peak are only a few MHz. Thus we can produce a probe beam through frequency offset generation from the pump beam. With frequency offset generation, the relative frequency is produced electronically, which allows the offset frequency to be specified much more accurately than with the heterodyne approach we used previously. This increase in accuracy improves the stability and linearity of the Rayleigh scans and eliminates the sign ambiguity using heterodyne measurements to determine the offset frequency between the two lasers. Near degeneracy, where the two wavelengths are almost equal, there can be ambiguity regarding which laser has the higher frequency.

We have attempted to measure the stimulated Rayleigh peak using offset modulation. Initially, the signal-to-noise ratio was not good because of the lower amount of power available in a single spatial mode from the external cavity diode laser. To enhance the signal-to-noise ratio, we performed homodyne detection of the stimulated scattering signal using a frequency mixer driven at the same frequency as the offset modulator. We observed a signal that was only present when the probe beam, pump beam, and offset modulation were present simultaneously, which was strong evidence that we had observed a signal from direct offset modulation. Definitive evidence would come from acquiring a stimulated Rayleigh scattering spectrum. Unfortunately, when we scanned the modulation frequency, we found large electrical interferences that prevented continuous acquisition of the signal. In addition, we found that the signal amplitude gradually changed between positive and negative values, an effect we tentatively attribute to the influence of the pump laser power on the refractive index generated by the stimulated scattering effect, which would be translated from the optical phase to the electrical phase in the frequency mixer.

To increase the available power single frequency, SRI has purchased an optical amplifier (Keopsys model KPS-BT2-SLM-YFA-04-PM-FA). This device uses a single mode polarization maintaining ytterbium fiber amplifier to produce up to 400 mW of output power. Using this amplifier to amplify the single frequency output of our master oscillator / laser provides two advantages. First, it yields a higher power for the probe beam derived from the master oscillator. This higher power increases the signal-to-noise ratio of the detected signal allowing us to monitor gains on the probe beam without using homodyne RF detection. Second, it provides a higher input power to the pulsed amplifier used to create the pump signal, reducing the possibility of parasitic oscillations.

We have performed experiments demonstrating the FM stimulated Rayleigh scattering technique using the fiber amplifier (Fig. 10). One portion of the amplified output is pulse-amplified using the apparatus shown in Fig. 8 to serve as the pump laser. The other portion is passed through a fiber-coupled phase modulator (Photline Technologies NIR-MPX-LN-10-P-P-FA-FA 10 GHz $LiNb0_3$ phase modulator for the for 1000 nm region). The modulation is scanned using an RF generator (HP model 8656B signal generator). The light is detected using a high-speed InGaAs photodiode (ThorLabs model SIR5). When the modulation frequency matches the offset frequency of the Rayleigh peak, a net signal will be produced on the optical wave at that frequency at the detector.

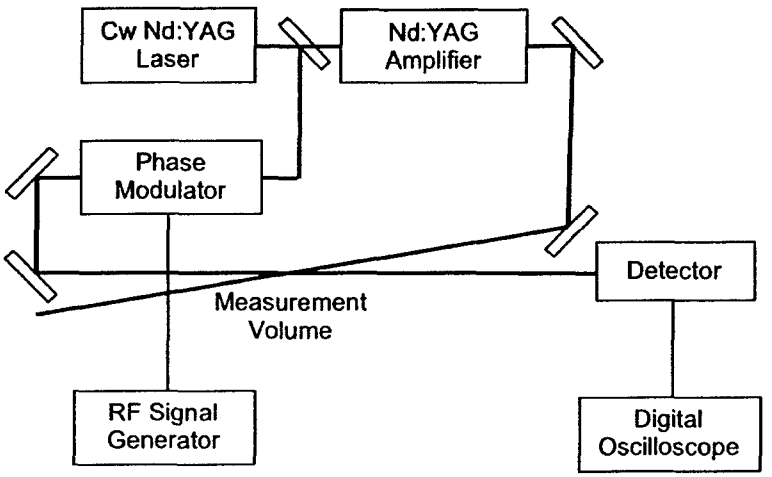

Figure 10. Schematic of pulsed stimulated scattering measurement with FM detection.

The resulting FM modulated signal is not phase locked to the RF drive signal because the phase modulator brings the RF phase up to the optical frequency, which is sensitive to changes in optical path length, similar to an interferometer. If we try to detect the FM signal through homodyne detection in a RF mixer, then small optical path length changes result in changes in the demodulated RF phase. Because of this RF phase drift, the RF amplitude cannot be measured using a single RF mixer.

We measure the RF amplitude by amplifying the detector output using two stages of low-noise amplifiers (Minicircuits model ZFL-500LN) and a digital oscilloscope. A fast-Fourier transform is performed on the oscilloscope, and the peak at the RF drive frequency is transferred to a PC through GPIB control. The PC also controls the RF generator through GPIB. A measurement of the stimulated Rayleigh peak was obtained by scanning the RF drive frequency while monitoring the oscilloscope Fourier transform peak at the same frequency. A measurement

of the stimulated Rayleigh peak is shown in Figure 11. The results of Fig. 11 and the two-laser scan in Fig. 1 show a number of distinctions. One of the differences is due to the nature of the FM modulation experiment, which provides a signal for only positive frequencies. Both the positive and negative peaks of the stimulated Rayleigh peak interact with the two sidebands of the FM modulated probe beam. These two sidebands cancel when the probe power is detected, leading to a single peak. Since we perform measurements in the linear range, the contributions of the two sidebands add, doubling the size of the signal. Two other differences are attributable to shortcomings of the current experiment. First, the signal of Fig. 11 has a square wave oscillation due to imperfect matching between the scan rate of RF generator frequency and the scan rate of the oscilloscope FFT readout frequency and the discrete nature of the FFT transformation.

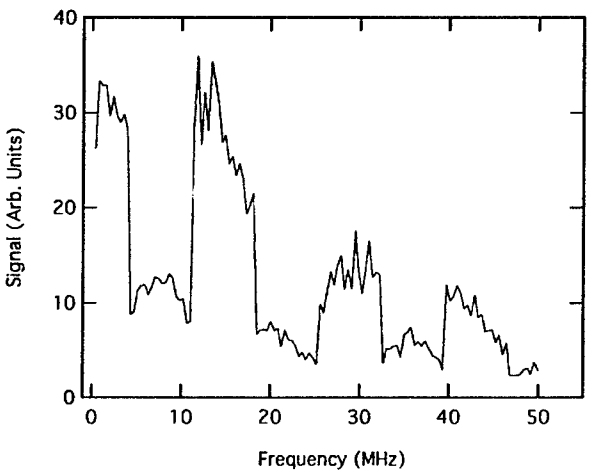

Figure 11. Stimulated Rayleigh signal acquired using FM modulation.

We have improved the results though a number of experimental changes. We added an additional optical isolator to eliminate feedback between the pulse amplified pump and the tunable diode laser. We matched the data acquisition interval to the oscilloscope Fourier transform interval to eliminate the square-wave oscillation of Fig. 11. Finally, we added an acoustooptic modulator to break the sideband symmetry of the phase modulator. The result, shown in Fig. 12, demonstrates the ability to perform frequency offset detection of the stimulated Rayleigh peak, opening the possibility of doing similar measurements in the supercritical regime.

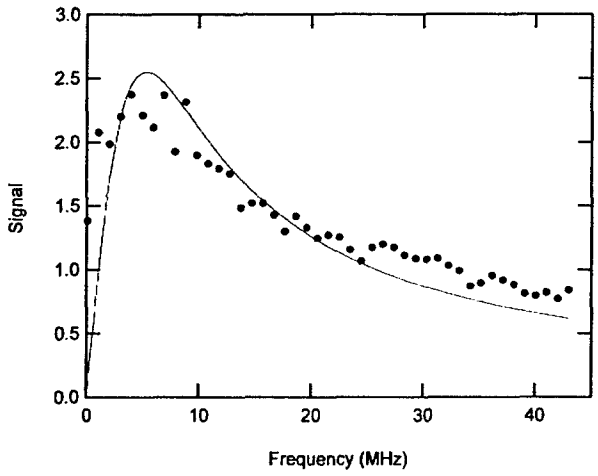

Fig. 12. Stimulated Rayleigh scattering in hexane. Data was acquired using double-pass two-stage amplification of a cw 1064-nm laser to produce the pump beam and the combination of acousto-optic modulator and phase modulator offsets to produce a probe beam.

REFERENCES

1. T. Edwards, personal communication (1996).

2. H. Eichler, G. Enterlein, P. Glozbach, J. Munschau, and H. Stahl, "Power requirements and resolution of real-time holograms in saturable absorbers and absorbing liquids," Appl. Opt. **11**, 372-375 (1972).

3. H. Eichler, G. Salje, and H. Stahl, "Thermal diffusion measurements using spatially periodic temperature distributions induced by laser light," J. Appl. Phys. **44**, 5383-5388 (1973).

4. D. W. Pohl, S. E. Schwarz, and V. Irniger, "Forced Rayleigh scattering," Phys. Rev. Lett. **31**, 32-35 (1973).

5. D. E. Govoni, J. A. Booze, A. Sinhal, and F. F. Crim, "The non-resonant signal in laser-induced grating spectroscopy of gases," Chem. Phys. Lett. **216**, 525-529 (1993).

6. S. Williams, L. A. Rahn, P. H. Paul, J. W. Forsman, and R. N. Zare, "Laser-induced thermal grating effects in flames," Opt. Lett. **19**, 1681-1683 (1994).

7. M. S. Brown, Y. Y. Li, W. L. Roberts, and J. R. Gord, "Analysis of transient-grating signals for reacting-flow applications," Appl. Opt. **42**, 566-578 (2003).

8. G. W. Faris, M. Gerken, C. Jirauschek, D. Hogan, and Y. Chen, "High-spectral-resolution stimulated Rayleigh–Brillouin scattering at 1 μm," Opt. Lett. **26**, 1894-1896 (2001).

9. M. B. Ewing and J. C. S. Ochoa, "Vapour pressures of n-hexane determined by comparative ebulliometry," J. Chem. Thermodyn. **38**, 283-288 (2006).

10. C. Jirauschek, E. M. Jeffrey, and G. W. Faris, "Electrostrictive and thermal stimulated Rayleigh spectroscopy in liquids," Phys. Rev. Lett. **87**, 233902 (2001).

11. K. Nishikawa and T. Morita, "Inhomogeneity of molecular distribution in supercritical fluids," Chem. Phys. Lett. **316**, 238–242 (2000).

12. H. Nakayama, K. Saitow, M. Sakashita, K. Ishii, and K. Nishikawa, "Raman spectral changes of neat CO_2 across the ridge of density fluctuation in supercritical region," Chem. Phys. Lett. **320**, 323-327 (2000).

13. G. W. Faris, M. J. Dyer, and W. K. Bischel, "Laser linewidth narrowing induced by amplifier gain saturation," Opt. Lett. **19**, 1529-1531 (1994).

PERSONNEL

The following personnel participated in the research supported by this contract:

Gregory W. Faris, Senior Physicist, principal investigator and lead experimentalist.

Xudong Xiao, Postdoctoral Fellow, experimentalist.

Kenneth T. Kotz, Postdoctoral Fellow, experimentalist.

Abneesh Srivastava, Research Scientist, experimentalist.

Steven Young, Mass Spectroscopy Specialist, electronics support.

William Olson, Engineering Assistant Mechanical, mechanical support.

David Watters, Program Director, consultant.

Andrei Knyazik, Summer Student, experimentalist.

Francisco Robles, Summer Student, experimentalist.

Erica Krivoy, Summer Student, experimentalist.

Mr. Knyazik, Mr. Robles, and Ms. Krivoy were supported by a Research Experiences for Undergraduates grant from the National Science Foundation.

PUBLICATIONS

This manuscript was submitted to the Journal of the Optical Society of America B. A copy is appended to this report.

Konstantinos S. Kalogerakis, Benjamin H. Blehm, Rachel E. Forman, Christian Jirauschek, and Gregory W. Faris, "Stimulated Rayleigh and Brillouin scattering in a supercritical fluid,"

INTERACTIONS/TRANSITIONS

PRESENTATIONS

G. W.Faris, "Advanced Stimulated Scattering Measurements in Supercritical Fluids," presented at ARO/AFOSR Contractors' Meeting in Chemical Propulsion, Tucson, AZ, 7-9 June, 2004.

K. T. Kotz, A. Knyazik, and G. W. Faris, "Diagnostics using stimulated Brillouin and Rayleigh scattering," Paper 5710-14, presented at Nonlinear Frequency Generation and Conversion: Materials, Devices, and Applications IV, Photonics West, San Jose, California, 22-27 January 2005.

K. S. Kalogerakis, B. H. Blehm, R. E. Forman, C. Jirauschek, and G. W. Faris, "Stimulated Rayleigh and Brillouin scattering in supercritical fluids," Paper JWA77, presented at Frontiers in Optics 2005, The 89th Optical Society of America Annual Meeting, Tucson, AZ, October 16-20, 2005.

INTERACTIONS

The following interactions occurred at the ARO/AFOSR Contractors Meeting in Chemical Propulsion, Williamsburg, Virginia, 23-25 June, 2003:

Tim Edwards, supercritical fuels, diagnostic requirements.

Timothy Lieuwen, acoustic measurements, Brillouin scattering.

Judy Wornat, supercritical diagnostics.

Jim Gord, lasers, diagnostics.

Mel Roquemore, miscellaneous research on combustion and fuels, ultrafast lasers.

Tom Jackson, high pressure and hypersonic diagnostics.

Paul Dimotakis, flow imaging.

Ron Hansen, laser diagnostics.

Fred Schauer, pulse detonation propulsion.

James Smith, hypergolic bipropellants, engines, diagnostics

Norm Laurendau, laser diagnostics, probability density functions.

The following interactions occurred at the ARO/AFOSR Contractors Meeting in Chemical Propulsion, Tucson, Arizona, 7-9 June 2004.

Tim Edwards, supercritical fuels, diagnostic requirements.

Jim Gord, complementary diagnostic techniques, novel diagnostics.

Mel Roquemore, miscellaneous topics.

Judy Wornat, supercritical diagnostics.

Ron Hansen, laser diagnostics.

Timothy Lieuwen, acoustic measurements, Brillouin scattering.

Cam Carter, topics in diagnostics.

Galen King, laser diagnostics, probability density functions.

Ajay Agrawal, beam deflection diagnostics.

Paul Dimotakis, supersonic flows and vortex formation.

Fred Schauer, pulse detonation propulsion.

James Smith, surface chemistry, hypergolic propellants, diagnostics, microfluidics.

The following interactions occurred at the ARO/AFOSR Contractors Meeting in Chemical Propulsion, Indianapolis, Indiana, 20-22 June 2005.

Tim Edwards, supercritical fuels, programmatic directions.

Ron Hansen, laser diagnostics.

Jim Gord, laser diagnostics and facilities.

Judy Wornat, supercritical fluid measurement techniques.

Ajay Agrawal, optical diagnostics.

Mel Roquemore, turbine engines.

Fred Schauer, pulse detonation propulsion.

Cam Carter, optical diagnostics.

Galen King, statistical measurements in turbulence, optical diagnostics.

Paul Dimotakis, high speed cameras.

Med Colket, trends in combustion research.

Ed Law, combustion chemistry.

Fred Gouldin, miscellaneous topics.

Norm Laurendau, diagnostics.

Bob Pitz, narrowband excimer lasers, diagnostics.

Steve Pope, miscellaneous topics.

Other Interactions

Martin Fejer, Stanford University, sensitive laser detection techniques.

David Watters, SRI, radio frequency detection techniques.

Jay Jeffries, Stanford University, diagnostic measurements.

Eric Lavelle, Jan Van Der Laan, Rich Schledewitz (all from SRI), Yves Deiss (Keopsys), Michelle Digonnet (Stanford University) – optical fiber techniques.

AIR FORCE RESEARCH LABORATORY INTERACTION

Our primary contact on this project at the Air Force Research Laboratory (AFRL) is Tim Edwards, with whom we have been communicating through email and at the AFOSR Contractor's Meetings. Tim has indicated that supercritical fuel thermal properties are an important need for the Air Force. Our original apparatus did not have sufficient spectral resolution to perform these measurements. In our recent work we have been modifying our apparatus to enable these measurements, including replacing the injection-seeded laser with a pulse amplified system and using electronic modulation to produce the probe beam instead of a two-laser system. Since we have successfully demonstrated stimulated Rayleigh scattering with these modifications, we are ready to perform supercritical fuel property measurements. We have also discussed with Cam Carter how these new diagnostic methods might be directly applicable at AFRL.

TRANSITIONS

None.

INVENTIONS/DISCOVERIES

SRI Invention Disclosure P5268 was filed on May 13, 2005. This disclosure describes electronic modulation methods for enhancing stimulated Brillouin and Rayleigh scattering and for performing sensitive absorption measurements.

HONORS/AWARDS

Gregory Faris

ARCS Fellow, 1985-1986

NSF Postdoctoral Fellow 1988-1989

Topical editor, *Applied Optics* 1999-2000

Associate editor, *Applied Optics* 2000-2004

2000-present Co-Director of NSF-sponsored Research Experiences for Undergraduates (REU) Program at SRI

1999-2000 Member, William F. Meggers Award Committee (Optical Society of America)

APPENDIX A
STIMULATED RAYLEIGH AND BRILLOUIN SCATTERING IN A SUPERCRITICAL FLUID

Stimulated Rayleigh and Brillouin scattering in a supercritical fluid

Konstantinos S. Kalogerakis, Benjamin H. Blehm, Rachel E. Forman,

Christian Jirauschek, and Gregory W. Faris

Molecular Physics Laboratory, SRI International

333 Ravenswood Avenue, Menlo Park, CA 94025

Abstract

We report stimulated Brillouin and Rayleigh scattering experiments in n-hexane for a wide range of sub- and supercritical temperature and pressure conditions, including the near-critical region. The measurements were performed in a cell designed for operation at conditions near or above the critical point. An injection-seeded Nd:YAG laser was employed as the pump laser and an external cavity diode laser as the probe laser. The use of 1064-nm light enhances stimulated Rayleigh scattering through direct thermal absorption. Analysis of the recorded spectra yielded the widths, shifts, and heights of the electrostrictive Brillouin, thermal Brillouin, and thermal Rayleigh peaks. Comparison of these features with theory has showed consistency with the theoretical predictions of the relationships between the heights and widths of the thermal Brillouin and thermal Rayleigh peaks. Remarkable structure and sudden changes in the behavior of the Brillouin shifts, widths, and heights were observed in the vicinity of the critical region.

OCIS Codes: 290.5900 Scattering, stimulated Brillouin; 290.5870 Scattering, Rayleigh; 190.1900 Diagnostic applications of nonlinear optics

1. Introduction

Supercritical fluids

Every substance has a thermodynamic critical point defined by a characteristic critical temperature and critical pressure. Below the critical point, there is a separation between liquid and gaseous phases. Above the critical point, this separation ceases to exist, and the fluid is called a supercritical fluid. Supercritical fluids have unusual properties that combine the properties of liquids and gases, with solubilities and densities similar to a liquid; and low viscosity, high diffusivity, and no surface tension similar to a gas. Because of these unusual properties, supercritical fluids are being applied as a solvent or reaction medium in a wide range of applications including chemical extraction and processing,[1] waste treatment,[2] and synthesis of nanomaterials.[3] Supercritical fluids are also relevant to advanced air-breathing propulsion systems where use of the fuel as a coolant can heat the fuel into the supercritical phase.[4] This paper describes investigations of supercritical fluids using stimulated scattering, which is described in the next section.

Simulated Scattering

Rayleigh, Brillouin, and Raman scattering occur commonly as spontaneous scattering. These scattering processes arise from natural oscillation modes of materials and can be used to determine the physical parameters responsible for these oscillations. When these collective modes are excited with a powerful laser, the mode oscillations can be driven so hard that they grow exponentially. This phenomenon is called stimulated scattering. The dominant advantage of stimulated scattering is that the scattered signal can be made arbitrarily large even though, otherwise, these processes spontaneously produce extremely weak signals. By using a probe to measure the induced amplification, we can obtain very good quantitative results. This technique is distinct from the stimulated scattering that builds up from noise, in which case quantification is very difficult.

The large signals from stimulated scattering are particularly helpful for investigating Rayleigh and Brillouin scattering, where the weak signals available from spontaneous scattering are difficult to discriminate from background excitation light. Other advantages of stimulated scattering include excellent temporal

resolution, and improved spectral resolution and signal-to-noise ratio. Furthermore, the use of two laser beams allows spatial registration and point measurement of local conditions.

The same pump-probe technique can be applied to all three processes—Rayleigh, Brillouin, and Raman. These processes together provide measurements of a wide range of material properties. Rayleigh scattering provides information on thermal properties, compositional fluctuations, and density; Brillouin scattering on compressional or elastic properties and density; and Raman scattering on chemical and compositional properties, density, and temperature.

Rayleigh scattering results from refractive index variations due to thermal waves or diffusive density fluctuations and compositional fluctuations. Brillouin scattering results from refractive index variations due to sound waves or traveling density or pressure fluctuations. These measurements may be performed at any wavelength for which the material is transparent. Generally, stimulated Rayleigh / Brillouin measurements are performed in the visible wavelength region using a ring dye laser, as has been applied to gases,[5,6] liquids,[6,7] and solids.[6,8] We have demonstrated that stimulated Rayleigh / Brillouin scattering may be performed quite well at a wavelength of 1064 nm using a tunable diode laser as a probe.[9,10] An advantage of performing measurements at this wavelength is the strong enhancement of the stimulated Rayleigh scattering peak in most liquids produced through optical absorption at vibrational overtone or combination bands.

Spontaneous Brillouin[11] and Raman[12-16] scattering have been applied to supercritical fluids. Transient grating techniques have also been applied to supercritical fluids.[17] In this paper, we report stimulated Brillouin and Rayleigh scattering experiments in n-hexane for a wide range of sub- and supercritical temperature and pressure conditions, including measurements in the near-critical region. To our knowledge, these are the first stimulated Rayleigh and stimulated Brillouin scattering in supercritical conditions. In the vicinity of the critical point, the observed scattering behavior exhibits remarkable structure and discontinuity.

2. Experiment

The experimental apparatus for stimulated Rayleigh and Brillouin scattering, shown schematically in Figure 1, has been described in detail previously.[9,10] For the optical arrangement, the pump laser is an injection seeded Nd:YAG laser. The linewidth of the pump laser is decreased by lowering the oscillator pump energy. This leads to longer pulsewidths with transform-limited linewidths of approximately 10 MHz. The probe laser is a tunable external cavity diode laser. The two lasers are overlapped in the sample cell in a counter-propagating geometry. The pump laser sets up an electric polarization oscillating at the characteristic frequency of a scattering mode of the material. For an intense input laser pulse, this polarization acts as a driving force, leading to amplification of both the material oscillation and a scattered optical wave. The optical amplification is detected as a gain or loss on the probe beam. The overlap volume of the pump and probe beams determines the spatial resolution. To reduce scattered light, the measurement cell windows are tilted slightly and the probe light is spatially filtered through an optical fiber. The probe laser wavelength is measured using a Fizeau wavemeter. Because of the narrow linewidths of the Rayleigh peak, transient effects can play an important role. We avoid the influence of such transient effects by using the time-integrated gain signal.[6,9]

The supercritical cell, shown in Figure 2, comprises two windows separated by an internal length of 2.5 cm. The windows are sealed using graphite rings. Titanium bolts are used on the flanges holding the windows because titanium has nearly the same thermal expansion coefficient as the glass windows. The cell, made of stainless steel, has been tested to temperatures as high as 600 °C and pressures as high as 14 MPa. Details of the high-pressure manifold are shown in Figure 3. High pressures are produced using a syringe pump. The temperature is actively controlled using a thermocouple and resistive heater. Secondary windows were placed at the ends of the heater to minimize convection from perturbing the laser beams. Most of the measurements were performed above the autoignition temperature of hexane, so any leak would form a fire. Safety features of the system include a pressure relief chamber, a backup temperature controller, and a lexan

enclosure around all portions of the system containing high pressure. The pump and probe beams were passed directly through the lexan enclosure without adverse effects on the measurements.

3. Results and Discussion

Examples of stimulated Rayleigh / Brillouin scattering spectra measured in n-hexane near the critical temperature at three different pressures are shown in Fig. 4. The abscissa is the difference in frequency between the pump and probe lasers determined by the wavemeter. The gain signal is divided by the pump and probe laser intensities to compensate for intensity fluctuations in each laser. The outer two peaks are Brillouin peaks; the central pair of peaks is due to stimulated Rayleigh scattering. The Brillouin peaks to the left and right are gain and loss peaks, respectively. For the loss peak, power is transferred from the probe laser to the pump laser. Absorption by CH overtone or combination bands increases the size of the stimulated Rayleigh peak, that would be difficult to observe otherwise, and causes an asymmetry in the stimulated Brillouin peak due to the imaginary Lorentzian shape of the thermal Brillouin scattering.

We developed software to enable automated analysis of measured spectra to extract the widths, shifts, and heights of the electrostrictive Brillouin, thermal Brillouin, and thermal Rayleigh peaks. Appropriate lineshapes are used for each spectral feature. The electrostrictive Brillouin lineshape is described by the real part of the complex Lorentzian profile; the thermal Brillouin and Rayleigh lineshapes are described by the imaginary parts of a complex Lorentzian profile.[18] These lineshapes must be convolved with the approximately Gaussian lineshape of the pump laser to produce the measured lineshapes, resulting in the real and imaginary parts of the complex error function for the Brillouin and Rayleigh peaks, respectively, the former being the familiar Voigt profile. The Igor graphics program (Wavemetrics, Inc.) was used for the line fitting using the algorithm of Humlicek.[19,20] Theoretical fits are shown as the thicker lines in Fig 4. The theory properly describes observed features of the spectra including the asymmetry of the Brillouin peaks, the remarkably large size of the stimulated Rayleigh peak (due to stimulated thermal scattering), and the relative sizes of the stimulated thermal Rayleigh and Brillouin peaks as compared with the electrostrictive Brillouin peak.[9]

The critical point for n-hexane occurs at a pressure 30.3 bar and temperature of 234 °C.[21] Figures 5 and 6 present three-dimensional views of the Brillouin shifts and the Brillouin peak widths observed for n-hexane at 1064 nm in a wide range of temperature and pressure conditions. In both graphs, an open circle on the temperature-pressure coordinate plane indicates the location of the critical point for n-hexane. The solid points correspond to the extracted values from our fits to the data, using the analysis procedure described earlier. In both graphs, the scatter of the data points is representative of the experimental uncertainties. The uncertainty of the fit (one standard deviation) is typically 1% and 5% for the Brillouin shift and Brillouin peak width. However, repeated measurements at the same conditions show a reproducibility to within approximately 10% and 20% for the Brillouin shift and width, respectively. The main source of experimental errors is the (unavoidable) existence of temperature and pressure fluctuations of the fluid under study, especially in the vicinity of the critical point. Our experiments for conditions ranging from ambient temperature and pressure to the supercritical state have clearly shown that these fluctuations become dramatically larger as the system approaches the critical point. The mesh surfaces shown in Figs. 5 and 6 have been created by numerical interpolation through the experimental points using commercially available software (Sigmaplot by SPSS Inc.). They are presented as a visual aid to the identification of trends in the experimental data. In both Figs. 5 and 6, the magnitude of the Brillouin shift and width exhibits a minimum in the region of the critical point. This observation is consistent with extreme values of the speed of sound and the acoustic damping rate attained near or at the critical point. Both the speed of sound and the damping rate are expected to approach zero in this region, which would correspond to the Brillouin shift and Brillouin width also approaching zero. We note that although our apparatus is successful in recording reliable spectra very close to the critical point, a limit exists within approximately a couple of bar and degrees C where critical opalescence and fluid fluctuations make measurements impossible. Consequently, the magnitude of the Brillouin shift and width could reach smaller values than those measured and approach zero at the critical point. Experiments with Raman scattering have shown the presence of ridge of large density fluctuation in the supercritical region.[15] We see evidence of such a

ridge in the slope discontinuities of Figs. 5 and 6. More experiments and analysis are required to clarify this behavior.

Figures 7, 8, and 9 show two-dimensional cross sections through the graphs of Figs. 5 and 6, and thus present a closer view of the behavior of the Brillouin shift and Brillouin peak width as a function of temperature and pressure. The error bars shown for the Brillouin width correspond to one standard deviation, as extracted from the fits to the data. In the case of the Brillouin shift the error bars from the fit to the data are comparable to the size of the point markers. As already mentioned, the main source of experimental error is fluctuations in the experimental conditions. Fig. 7 shows the minima of the Brillouin shift and Brillouin width near the critical point more clearly. Fig. 8 shows the general rise in the shift and width as temperature decreases toward the critical temperature above the critical pressure. Fig. 9 shows that the minimum in the Brillouin shift and Brillouin width at the critical pressure persists above the critical temperature.

Figure 10 shows results from analysis of the intensities of the stimulated Brillouin peaks. The extraction of information from the intensity of the data presents special challenges: The data must be (1) recorded under very similar or ideally identical conditions for the signal integration, (2) normalized for the intensity of the pump and probe lasers, and (3) corrected for the dependence of the fluid number density on the experimental conditions. Despite the greater difficulty associated with the determination of accurate and properly normalized peak intensities, the trends shown in the data of Fig. 10 is noteworthy. Both the absorptive and the electrostrictive components of the Brillouin scattering peak show a sharp discontinuity near the critical point. This is expected because the near critical fluid is very susceptible to density fluctuations such as are induced by stimulated Brillouin scattering. The same trend occurs in the absorptive component. In the experiments, we found that the magnitude of the absorptive component of the stimulated Brillouin scattering peak for n-hexane at 1064 nm was not more than 10% of the electrostrictive component's magnitude.

In summary, we have applied stimulated Rayleigh and Brillouin scattering to supercritical hexane including the near critical region. Detailed information on the Brillouin widths, shifts, and heights are obtained.

Unusual behavior is found in the supercritical region, including enhanced stimulated Brillouin peak heights and local minima in the Brillouin shifts and widths. Improvements in the pump laser linewidth will be required to perform accurate measurements of the Rayleigh linewidth in the supercritical region as the linewidths are narrower than for the subcritical liquid.[9] We plan to use a pulse-amplified laser to resolve the supercritical Rayleigh line in future work.

4. Acknowledgments

This work was supported by the Air Force Office of Scientific Research under contracts F49620-01-C-0020 and F49620-03-C-0015. R.E. Forman and B.H. Blehm were supported by the Research Experiences for Undergraduates program of the National Science Foundation (Grant PHY-0097861).

5. References

1. R. Noyori, "Supercritical Fluids: Introduction," Chem. Rev. **99,** 353-354 (1999).
2. P. Kritzer and E. Dinjus, "An assessment of supercritical water oxidation (SCWO) - Existing problems, possible solutions and new reactor concepts," Chemical Engineering Journal **83,** 207-214 (2001).
3. R. A. Pai, R. Humayun, M. T. Schulberg, A. Sengupta, J. N. Sun, and J. J. Watkins, "Mesoporous silicates prepared using preorganized templates in supercritical fluids," Science **303,** 507-510 (2004).
4. T. Edwards, "Cracking and deposition behavior of supercritical hydrocarbon aviation fuels," Combust. Sci. Technol. **178,** 307-334 (2006).
5. S. Y. Tang, C. Y. She, and S. A. Lee, "Continuous-wave Rayleigh-Brillouin-gain spectroscopy in SF_6," Opt. Lett. **12,** 870-872 (1987).
6. G. W. Faris, L. E. Jusinski, and A. P. Hickman, "High-resolution stimulated Brillouin gain spectroscopy in glasses and crystals," J. Opt. Soc. Am. B **10,** 587-599 (1993).
7. K. Ratanaphruks, W. T. Grubbs, and R. A. MacPhail, "CW stimulated Brillouin gain spectroscopy of liquids," Chem. Phys. Lett. **182,** 371-378 (1991).
8. G. W. Faris, L. E. Jusinski, M. J. Dyer, W. K. Bischel, and A. P. Hickman, "High-resolution Brillouin gain spectroscopy in fused silica," Opt. Lett. **15,** 703-705 (1990).
9. G. W. Faris, M. Gerken, C. Jirauschek, D. Hogan, and Y. Chen, "High-spectral-resolution stimulated Rayleigh–Brillouin scattering at 1 μm," Opt. Lett. **26,** 1894-1896 (2001).
10. C. Jirauschek, E. M. Jeffrey, and G. W. Faris, "Electrostrictive and thermal stimulated Rayleigh spectroscopy in liquids," Phys. Rev. Lett. **87,** 233902 (2001).
11. R. W. Gammon, H. L. Swinney, and H. Z. Cummins, "Brillouin scattering in carbon dioxide in the critical region," Phys. Rev. Lett. **19,** 1467-1469 (1967).
12. M. S. Brown and R. R. Steeper, "CO_2-based thermometry of supercritical water oxidation," Appl. Spectrosc. **45,** 1733-1738 (1991).

13. W. Kohl, H. A. Lindner, and E. U. Franck, "Raman spectra of water to 400 °C and 3000 bar," Ber. Bunsenges. Phys. Chem. **95,** 1586-1593 (1991).

14. M. Oschwald and A. Schik, "Supercritical nitrogen free jet investigated by spontaneous Raman scattering," Experiments In Fluids **27,** 497-506 (1999).

15. H. Nakayama, K. Saitow, M. Sakashita, K. Ishii, and K. Nishikawa, "Raman spectral changes of neat CO_2 across the ridge of density fluctuation in supercritical region," Chem. Phys. Lett. **320,** 323-327 (2000).

16. A. Idrissi, S. Longelin, P. Damay, and F. Leclercq, "Low-frequency Raman spectra of sub- and supercritical CO_2: Qualitative analysis of the diffusion coefficient behavior," J. Chem. Phys. **123,** (2005).

17. E. H. Abramson and J. M. Brown, "Equation of state of water based on speeds of sound measured in the diamond-anvil cell," Geochim. Cosmochim. Acta **68,** 1827-1835 (2004).

18. W. Kaiser and M. Maier, "Stimulated Rayleigh, Brillouin, and Raman spectroscopy," in Laser Handbook, edited by F. T. Arecchi and E. O. Schulz-Dubois (North-Holland, Amsterdam, 1972), Vol. 2, pp. 1077-1150.

19. J. Humlicek, "Optimized computation of the Voigt and complex probability functions," J. Quant. Spectrosc. Radiat. Transfer **27,** 437-444 (1982).

20. F. Schreier, "The Voigt and complex error function: A comparison of computational methods," J. Quant. Spectrosc. Radiat. Transfer **48,** 743-762 (1992).

21. M. B. Ewing and J. C. S. Ochoa, "Vapour pressures of n-hexane determined by comparative ebulliometry," J. Chem. Thermodyn. **38,** 283-288 (2006).

Figure Captions

Fig. 1. Schematic of experimental apparatus for stimulated Rayleigh and stimulated Brillouin scattering.

Fig. 2. Schematic of supercritical cell design.

Fig. 3. Schematic of high-pressure manifold.

Fig. 4. (Color Online) Stimulated Rayleigh / Brillouin scattering spectrum for n-hexane measured at 1064 nm near the critical temperature (247 °C) for three different pressures. The spectral fits to the data including the electrostrictive and thermal components to the fit are shown as thick lines.

Fig. 5. The Brillouin shift (solid circles) observed in stimulated Brillouin scattering for n-hexane at 1064 nm as a function of temperature and pressure. The location of the critical point is shown by the open circle.

Fig. 6. The Brillouin peak width (solid circles) observed in stimulated Brillouin scattering for n-hexane at 1064 nm as a function of temperature and pressure. The location of the critical point is shown by the open circle.

Fig. 7. The Brillouin (a) shift and (b) width observed in stimulated Brillouin scattering for n-hexane at 1064 nm as a function of pressure for a temperature of 233.6 °C. Both the Brillouin shift and width have a local minimum near the critical point.

Fig. 8. The Brillouin (a) shift and (b) width observed in stimulated Brillouin scattering for n-hexane at 1064 nm for a pressure of 45 bar as a function of temperature. Local maxima are observed near the critical temperature above the critical pressure.

Fig. 9. The Brillouin (a) shift and (b) width for n-hexane at 240 °C as a function of pressure.

Fig. 10. The intensity of the electrostrictive and absorptive components of stimulated Brillouin scattering for n-hexane at 1064 nm for a temperature of 232 ° C as a function of pressure. A sharp increase in intensity is observed near the critical point.

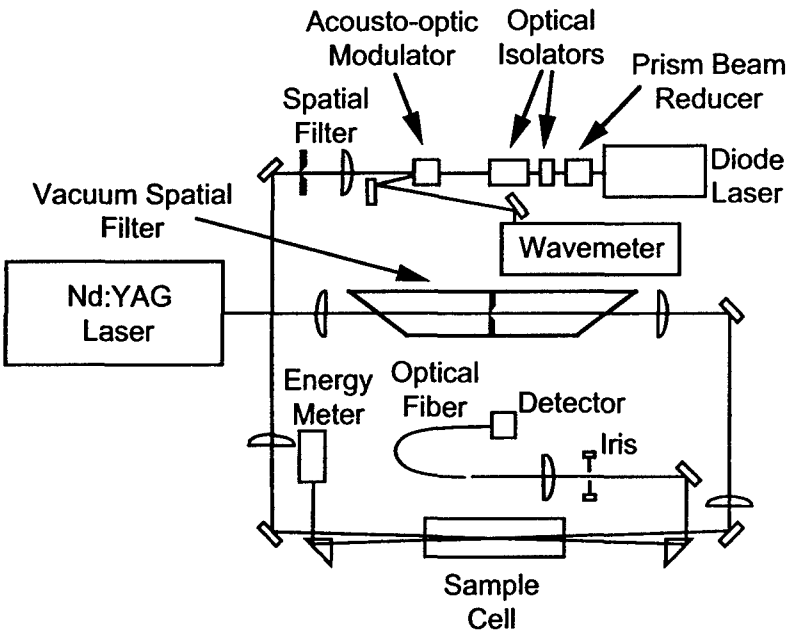

Fig. 1. Schematic of experimental apparatus for stimulated Rayleigh and stimulated Brillouin scattering.

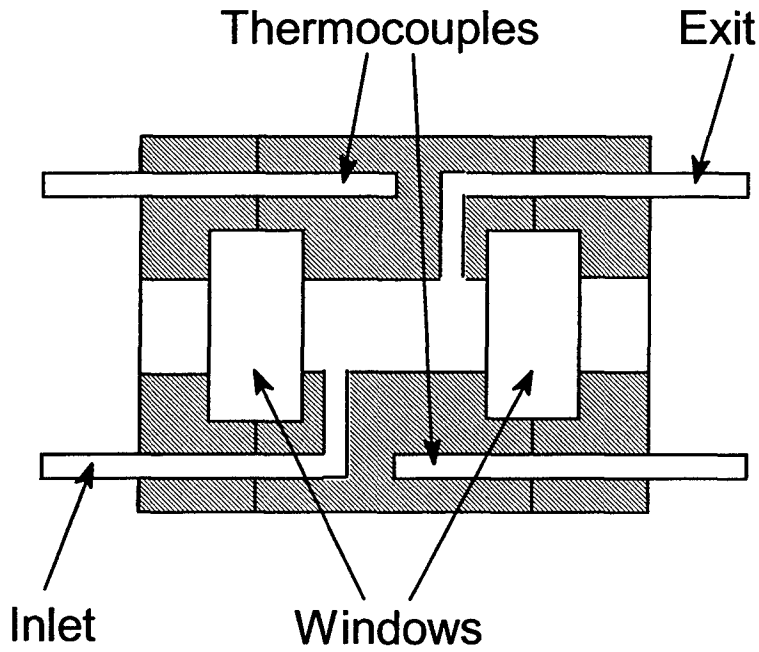

Fig. 2. Schematic of supercritical cell design.

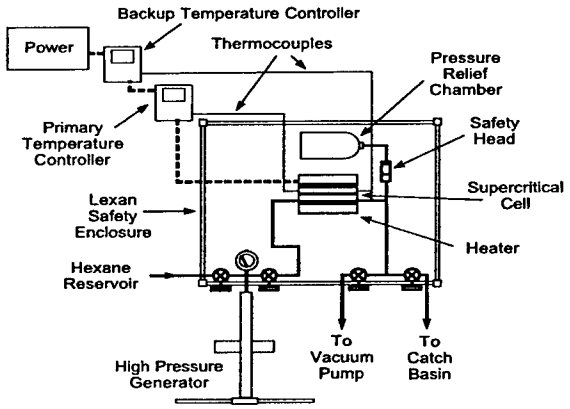

Fig. 3. Schematic of high-pressure manifold.

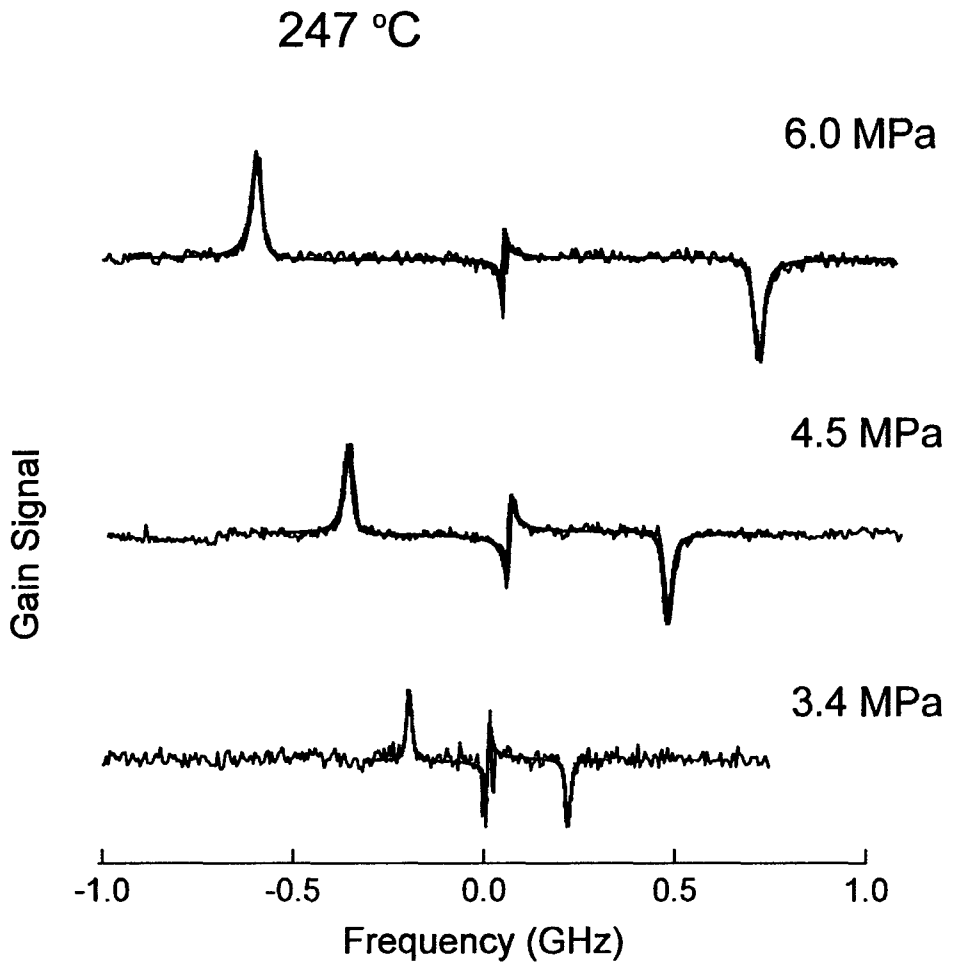

Fig. 4. (Color Online) Stimulated Rayleigh / Brillouin scattering spectrum for n-hexane measured at 1064 nm near the critical temperature (247 °C) for three different pressures. The spectral fits to the data including the electrostrictive and thermal components to the fit are shown as thick lines.

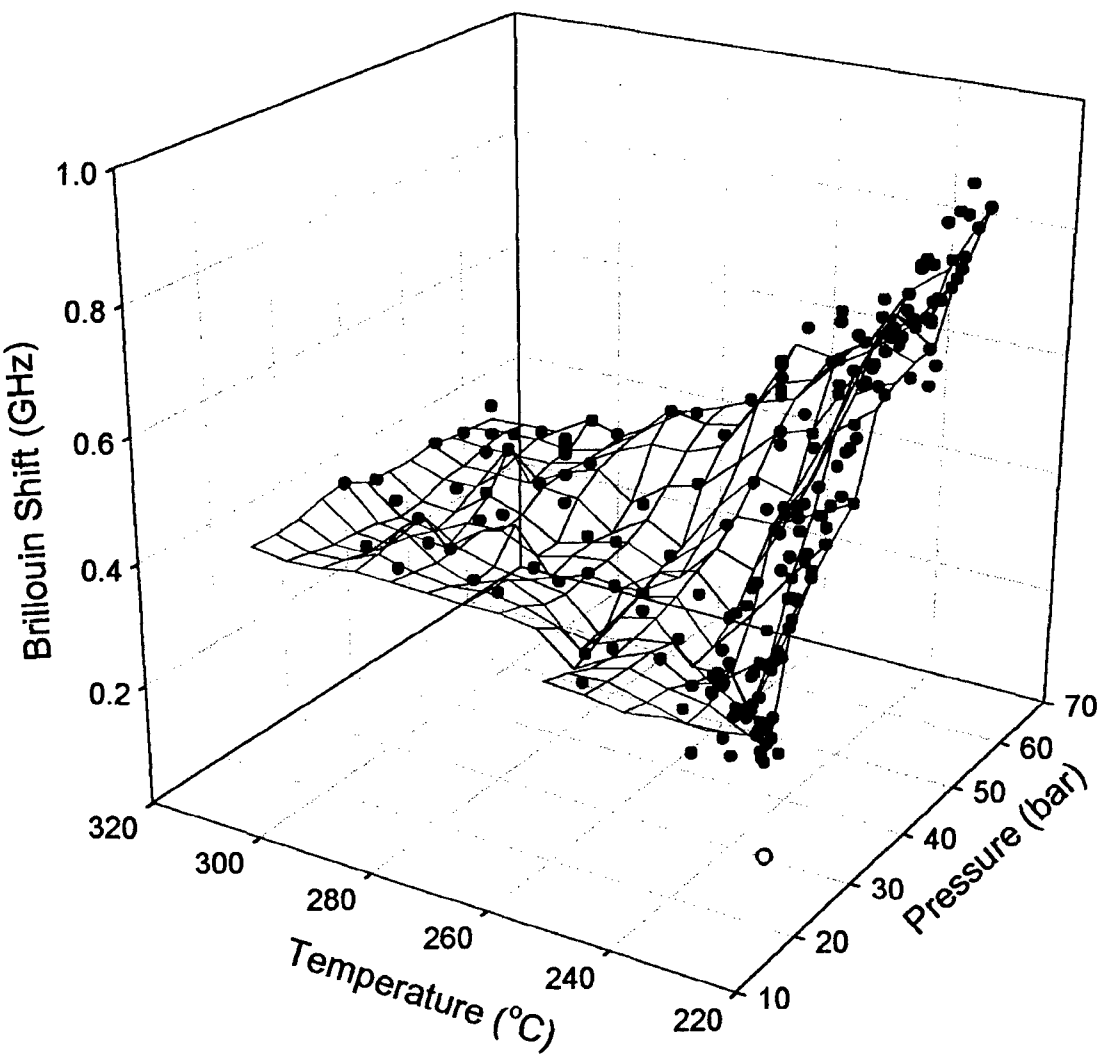

Fig. 5. The Brillouin shift (solid circles) observed in stimulated Brillouin scattering for n-hexane at 1064 nm as a function of temperature and pressure. The location of the critical point is shown by the open circle.

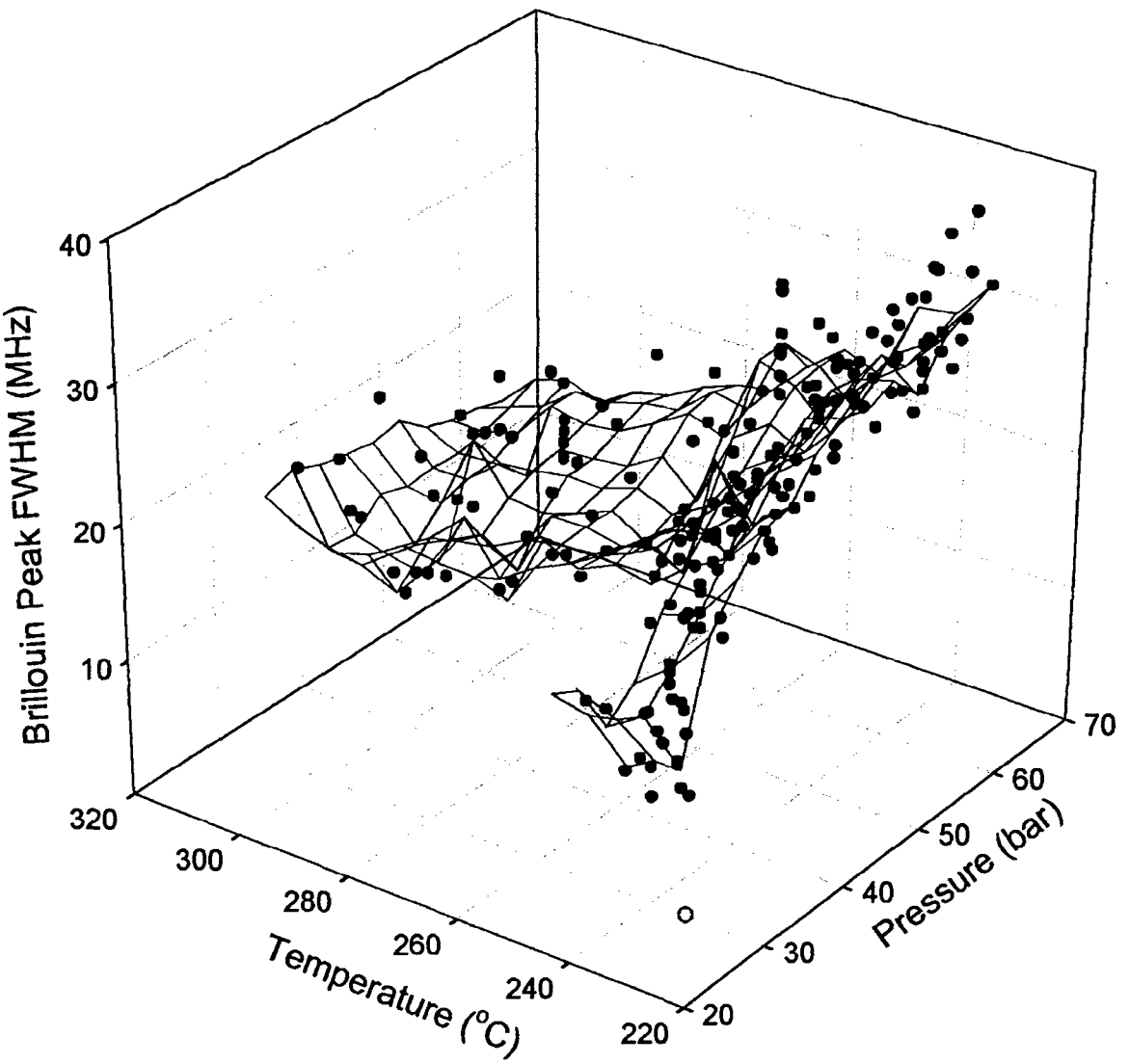

Fig. 6. The Brillouin peak width (solid circles) observed in stimulated Brillouin scattering for n-hexane at 1064 nm as a function of temperature and pressure. The location of the critical point is shown by the open circle.

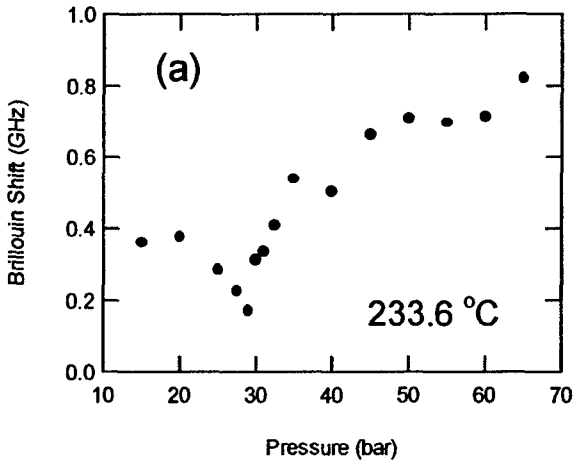

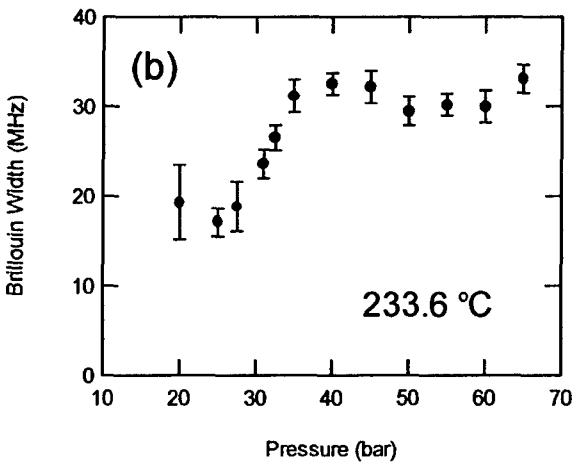

Fig. 7. The Brillouin (a) shift and (b) width observed in stimulated Brillouin scattering for n-hexane at 1064 nm as a function of pressure for a temperature of 233.6 °C. Both the Brillouin shift and width have a local minimum near the critical point.

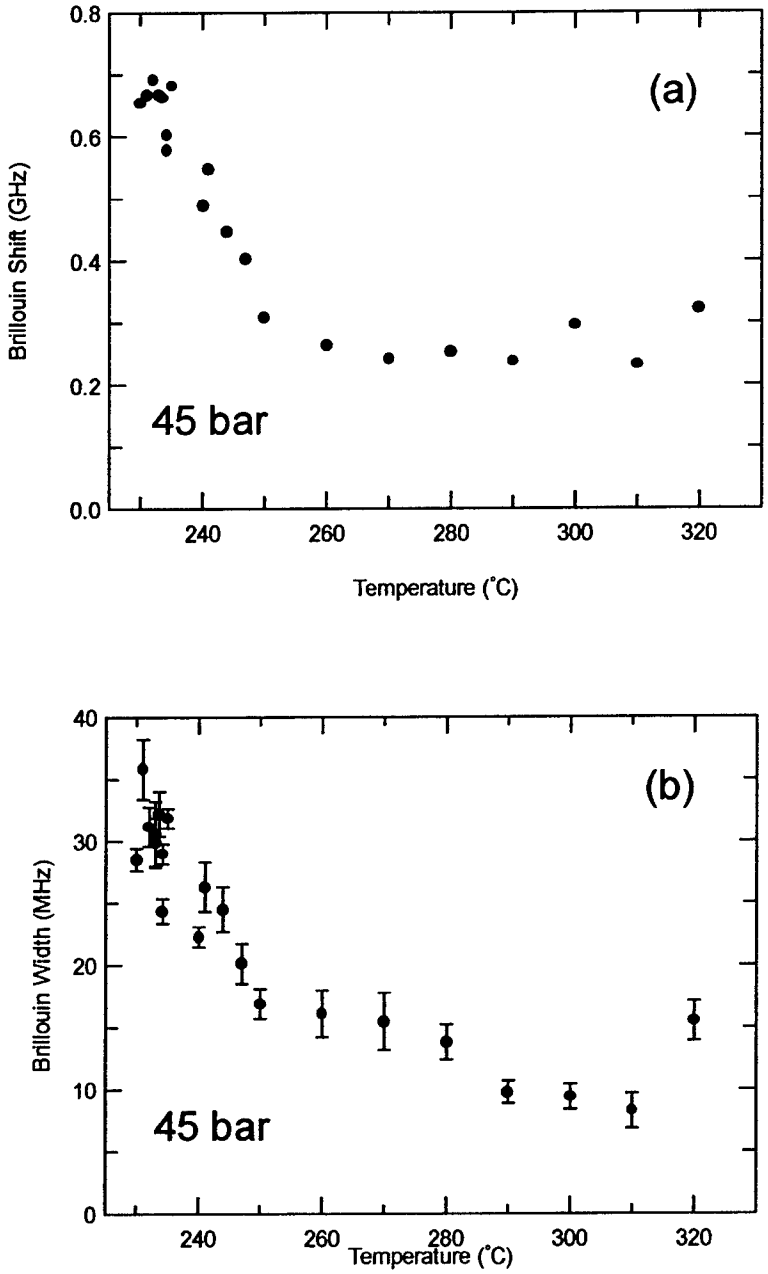

Fig. 8. The Brillouin (a) shift and (b) width observed in stimulated Brillouin scattering for n-hexane at 1064 nm for a pressure of 45 bar as a function of temperature. Local maxima are observed near the critical temperature above the critical pressure.

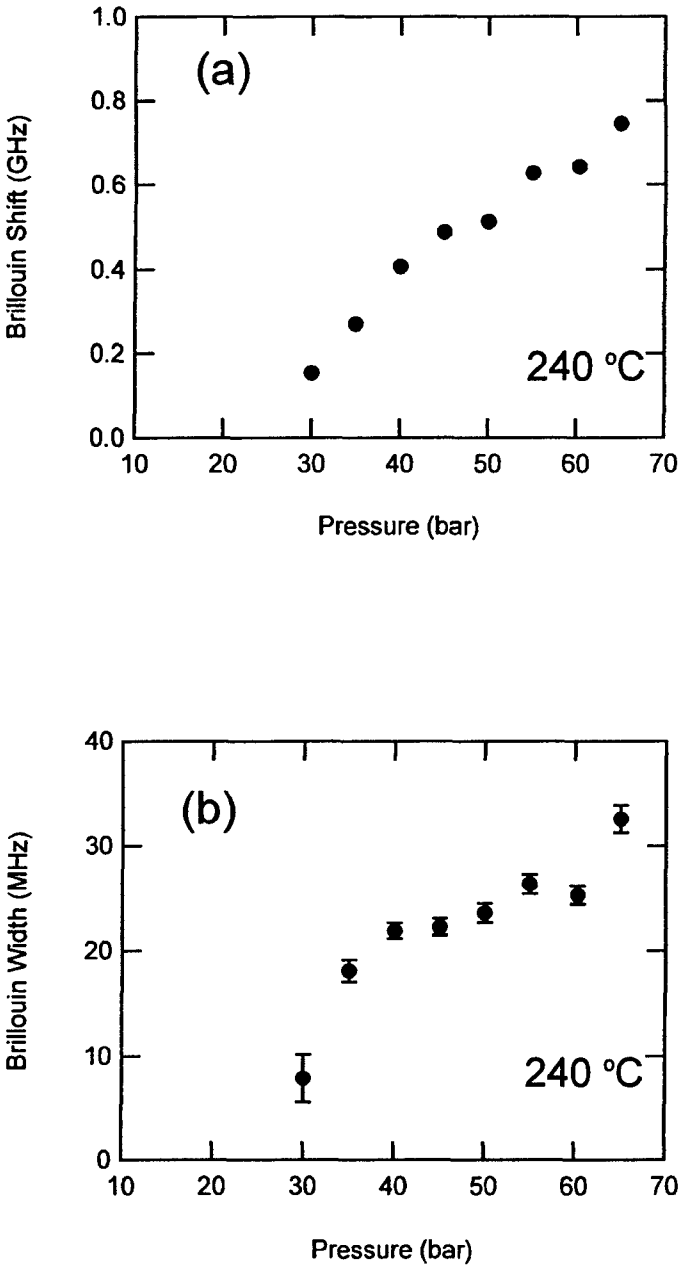

Fig. 9. The Brillouin (a) shift and (b) width for n-hexane at 240 °C as a function of pressure.

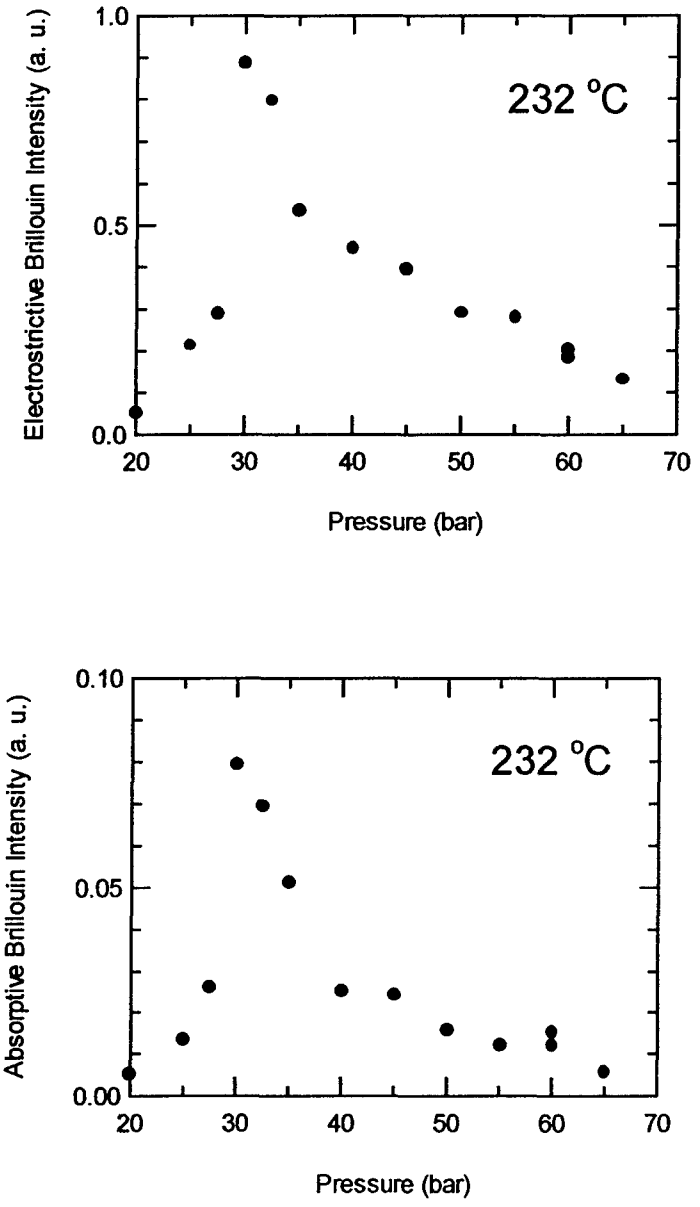

Fig. 10. The intensity of the electrostrictive and absorptive components of stimulated Brillouin scattering for n-hexane at 1064 nm for a temperature of 232 °C as a function of pressure. A sharp increase in intensity is observed near the critical point.